



# Performance and mechanism of CuO/CuZnAl hydrotalcites-ZnO for photocatalytic selective oxidation of gaseous methanol to methyl formate at ambient temperature



Xiaoyuan Liang<sup>a</sup>, Xuzhuang Yang<sup>a,\*</sup>, Guanjun Gao<sup>a</sup>, Changfu Li<sup>a</sup>, Yuanyuan Li<sup>a</sup>, Weida Zhang<sup>a</sup>, Xuetao Chen<sup>a</sup>, Yanbing Zhang<sup>a</sup>, Bingbing Zhang<sup>a</sup>, Yanqiu Lei<sup>a</sup>, Quanquan Shi<sup>b</sup>

<sup>a</sup> School of Chemistry and Chemical Engineering, Inner Mongolia University, Hohhot, Inner Mongolia 010021, People's Republic of China

<sup>b</sup> State Key Laboratory of Catalysis, Dalian Institute of Chemical Physics, Chinese Academy of Sciences, Dalian 116023, People's Republic of China

## ARTICLE INFO

### Article history:

Received 20 February 2016

Revised 28 March 2016

Accepted 29 March 2016

### Keywords:

Photocatalysis

Methanol

Methyl formate

Copper catalyst

Reaction mechanism

## ABSTRACT

The photocatalytic selective oxidation of methanol to methyl formate at 26–45 °C under UV irradiation has been studied for the first time on the catalyst CuO supported on nanocomposites of CuZnAl hydrotalcites and ZnO. The catalyst exhibits high activity for this reaction, with a maximum methyl formate yield of 50% at 30 °C and no by-product other than CO<sub>2</sub>, although both ZnO and hydrotalcites are nonactive for the reaction. The interfaces between ZnO and CuZnAl hydrotalcites play an important role in the reaction, not only supplying necessary hydroxyls but also generating holes with redox potential positive enough for the reaction under UV irradiation due to the band bending at the interface. Copper oxide is photoreduced to metallic Cu during the reaction, which plays a role in trapping photoexcited electrons from the conduction band of the support as well as in dissociating chemisorbed oxygen.

© 2016 Elsevier Inc. All rights reserved.

## 1. Introduction

Methyl formate (MF) is an important industrial intermediate for synthesizing formic acid, formamides, acetic acid, ethylene glycol, etc. [1–3]. It is traditionally produced by dehydrogenation (direct or oxidative) of methanol at elevated temperatures and/or pressures [1–5], leading to energy waste, multiple by-products, and low MF selectivity. Wittstock et al. reported selective oxidation of methanol to MF with high MF selectivity on nanoporous gold catalyst at low temperatures [6], which shed new light on green MF production. In recent years, photocatalytic MF synthesis from methanol has attracted great attention of researchers due to its ambient reaction conditions and high MF yield [7–11], Liu et al. reported photocatalytic methanol oxidation on MoO<sub>3</sub>/TiO<sub>2</sub> and TiO<sub>2</sub> as early as 1985, MF being one of the multiple products [12]. Kominami et al. studied this reaction on an anatase-type TiO<sub>2</sub> (ST-01) in 2010 [11]. We studied Au, Ag, Au–Ag alloy, and Cu nanoparticles supported on TiO<sub>2</sub> as photocatalysts for MF synthesis from methanol at 15–45 °C under UV irradiation [7–9]. Colmenares et al. reported that Pd–Au/TiO<sub>2</sub> as a photocatalyst was active in selective oxidation of methanol to MF [10]. Photocatalysts

other than titania are seldom used in photocatalytic oxidation of methanol to MF.

The band gap energy of ZnO is close to that of TiO<sub>2</sub>, and the valence band maximum and conduction band minimum of ZnO, which determine the redox potential under irradiation, are also similar to those of TiO<sub>2</sub> [13]. Thus, ZnO exhibits photocatalytic performance comparable or superior to that of TiO<sub>2</sub> in many cases, such as photodegradation of organics, water splitting, and photocatalytic conversion of CO<sub>2</sub> and CH<sub>4</sub> [14–20]. ZnO is becoming a promising photocatalyst instead of TiO<sub>2</sub> due to its low cost, high reactivity, and easy production [14,16]. But unlike TiO<sub>2</sub>, ZnO exhibited almost no any photocatalytic activity in the selective oxidation of methanol to MF [7]. The mechanism of the reaction indicates that hydroxyls on the surface of the catalyst are responsible for the key step of forming methoxyl from methanol [3,7,8], but there are much rarer surface hydroxyls on ZnO than on TiO<sub>2</sub>. It is still challenging to use ZnO or modified ZnO as a photocatalyst in photocatalytic oxidation of methanol to MF.

Zn and Al or Cu, Zn, and Al can form hydrotalcites, which are semiconductors with plenty of surface hydroxyls and have been used in many photocatalytic processes [21–27], but the valence band maximum of hydrotalcites is usually higher than that of ZnO [28], leading to more negative redox potential of the photoexcited holes and thus lower oxidation capacity. Some researchers

\* Corresponding author. Fax: +86 471 4992981.

E-mail address: [xzyang2007@yahoo.com](mailto:xzyang2007@yahoo.com) (X. Yang).

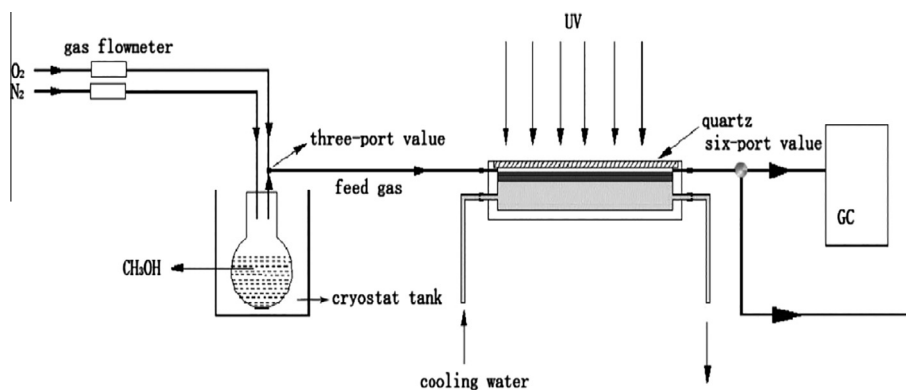


Fig. 1. Schematic diagram of the reaction process.

prepared semiconductors such as TiO<sub>2</sub> [29–32] or CeO<sub>2</sub> [33] – modified hydrotalcites for photocatalysis and achieved favorable results. The heterojunction between the semiconductor and hydrotalcites is considered to play a role in electron transfer and thus promote photocatalysis [31]. So preparation of highly efficient photocatalysts for selective oxidation of methanol to MF through the combination of ZnO and CuZnAl hydrotalcites is anticipated. The sites at the heterojunction close to the side of ZnO are expected to provide photogenerated holes with redox potential high enough for the reaction and those close to the side of hydrotalcites supply hydroxyls for the reaction.

Copper oxide is also a semiconductor with a band gap of ca. 1.7 eV [34,35]. It has been used as a photocatalyst for H<sub>2</sub> production [36–39], CO<sub>2</sub> reduction [40–45], organics degradation [46,47], etc. under visible light irradiation in recent years. However, copper oxide is unstable under irradiation because the redox potential for reduction and oxidation of monovalent copper oxide lies within its band gap [48–50] and thus it is easily photoreduced to metallic copper. This disadvantage of CuO turns into an advantage when it is supported on titania for photocatalytic oxidation of methanol to MF, because it can form an ohmic contact between metallic copper and titania, as the work function of copper is slightly lower than that of titania [8]. Such a structure facilitates charge transfer from titania to Cu nanoparticles and oxygen dissociation on Cu nanoparticles during the reaction. The work function of ZnO (bulk) is ca. 5.3 eV [51], which is higher than that of Cu ( $\varphi_{\text{Cu}} = 4.60$  eV [52,53]), and thus an ohmic contact might also be formed between Cu nanoparticles and ZnO. Actually, the work function of a metal or a semiconductor is not constant and changes with its morphology and size. An electronic contact between metal and semiconductor can form an ohmic contact or a Schottky barrier. Both are beneficial to charge separation under irradiation. In the case of ohmic contact, the photoexcited electrons are easy to transfer to the Cu nanoparticles due to the lower resistance at the interface between the Cu nanoparticle and the semiconductor, while in the case of Schottky contact the photoexcited electrons are trapped by Cu nanoparticles, which reduces the electron–hole recombination [54–59]. In addition, the negatively charged surfaces of Cu nanoparticles are beneficial for the dissociative chemisorption of oxygen molecules and thus conducive to the reaction [7,8].

In this study, we have prepared nanocomposites of CuO supported on CuZnAl hydrotalcites and ZnO by a two-step wet chemical method using simple precursors such as Zn(NO<sub>3</sub>)<sub>2</sub>·6H<sub>2</sub>O, Al<sub>2</sub>(SO<sub>4</sub>)<sub>3</sub>·18H<sub>2</sub>O, and Cu(NO<sub>3</sub>)<sub>2</sub> as an efficient photocatalyst for selective oxidation of methanol to MF at 26–45 °C under UV irradiation. The objectives of this study are to investigate the photocatalytic performance of the catalysts, the influence of methanol

partial pressure, oxygen partial pressure, and light intensity on photocatalysis, and the reaction mechanisms of the catalysts.

## 2. Experimental

### 2.1. Catalyst preparation

Typically, 7.425 g Zn(NO<sub>3</sub>)<sub>2</sub>·6H<sub>2</sub>O and a suitable amount of Al<sub>2</sub>(SO<sub>4</sub>)<sub>3</sub>·18H<sub>2</sub>O (molar ratio Al<sub>2</sub>O<sub>3</sub>/ZnO = 1%, 3%, 5%, 7%, 10%) were dissolved in 250 mL deionized water followed by adding 2 mL Triton X-100 under ultrasonic stirring for 0.5 h. A solution of 0.2 mol L<sup>-1</sup> Na<sub>2</sub>CO<sub>3</sub> was added dropwise under ultrasonic stirring until the above solution reached pH 8. Ultrasonic stirring was continued for 2 h. The precipitate was recovered after centrifugation, washing with deionized water and ethanol and drying in air. The nanocomposites of H-ZnO-y(z) were then obtained after calcination at different temperatures (300, 400, 500, 600, 700, and 800 °C) for 3 h, where H denotes the hydrotalcites, y denotes the Al loading, and z denotes the calcination temperature.

The as-prepared H-ZnO-y(z) nanocomposites of 0.2 g, where y denotes the Al loading and z denotes the calcination temperature of H-ZnO-y(z), were supersonically dispersed in a solution of 0.01 mol L<sup>-1</sup> Cu(NO<sub>3</sub>)<sub>2</sub> solution (molar ratio of Cu/Zn = 3%, 5%, 7%, and 10%) and deionized water (volumetric ratio of water to Cu(NO<sub>3</sub>)<sub>2</sub> solution is 10) for 25 min followed by adding 5 mL aqueous solution of NaBH<sub>4</sub> (molar ratio of Cu/NaBH<sub>4</sub> = 1/2.5) with vigorous stirring for 24 h. The solid recovered was dried at 50 °C in air after washing with deionized water and ethanol. The catalyst was labeled xCu/H-ZnO-y(z), where x denotes the Cu loading.

### 2.2. Catalyst characterization

X-ray diffraction (XRD) measurements were performed using a PANalytical B.V. Empyrean diffractometer with CuK $\alpha$  radiation operated at 40 kV and 40 mA. The scanning range ( $2\theta$ ) was 10–80°. The morphology of the samples was investigated by a FEI Tecnai S-Twin transmission electron microscopy (TEM). The light absorbance was measured by a UVIKON/XL UV–vis diffuse reflectance spectrometer (UV–vis) with a scanning range of 200–800 nm. Temperature-programmed reduction with hydrogen (H<sub>2</sub> TPR) was performed with a Micromeritics AutoChem 2910 analyzer. The gas mixture is 10% H<sub>2</sub> balanced with N<sub>2</sub> and the flow rate is 50 mL/min. The heating rate is 8 °C/min. A 20 mg sample was loaded into the quartz tube for each run. A Fourier transform infrared (FTIR) spectrum was recorded on a Bruker Vertex 70 FTIR spectrometer. A 20 mg sample was added into 200 mg KBr, followed by tablet compressing. In order to remove water absorbed in the cat-

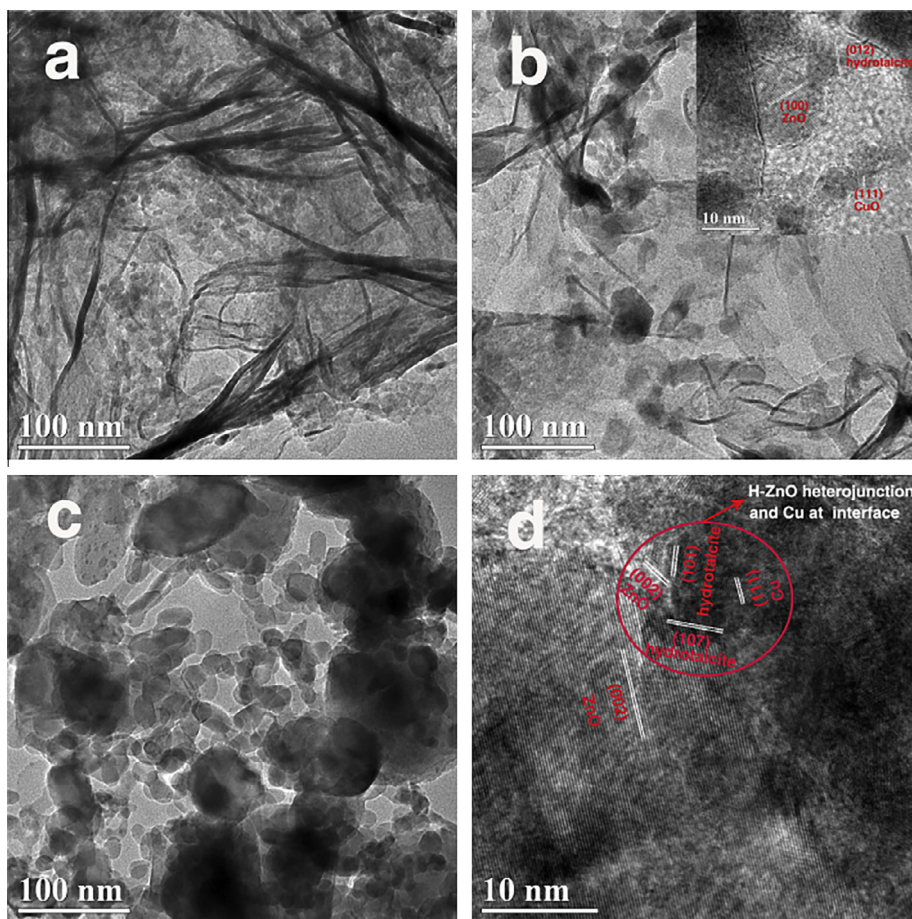


**Fig. 2.** TEM images of catalysts 7Cu/H-ZnO-5(3) (a), 7Cu/H-ZnO-5(7) (b), and 7Cu/H-ZnO-5(8) (c). HRTEM of used 7Cu/H-ZnO-5(7) obtained within 2 min after catalysis (d).

alysts, all samples were dried at 120 °C for 24 h before testing. The X-ray photoelectron spectra (XPS) of the catalysts were recorded by a Kratos Amicus spectrometer using an AlK $\alpha$  (1486.6 eV) radiation source. The binding energy (BE) was adjusted by the C1s transition at 284.6 eV.

### 2.3. Photocatalytic reaction

The photocatalytic activity of the catalyst was measured in a continuous-flow aluminum alloy reactor with a rectangular quartz window on top and a dividing-wall-type heat exchanger connected to the back at the bottom of the reactor. The schematic diagram of the reaction process can be seen in Fig. 1. Three pieces of rectangular glass coated with 0.02 g catalyst g on their top surfaces, which were used as the catalyst holders, were installed in the bottom of the reactor, with a thermocouple fixed in touch with the middle catalyst holder. The dimensions of each of the glass holders were 26 × 80 × 1 mm. The whole surface coated by catalyst can be irradiated by light. The cooling water flowed through the heat exchanger to maintain a constant temperature. A 500 W high-pressure mercury lamp (CEL-LAM500) with maximum light intensity at wavelength 365 nm was positioned in a quartz cooling jacket 2 cm over the quartz window of the reactor. The light intensity was 25.3 mW/cm<sup>2</sup>. A gas mixture containing 1.0 vol.% methanol and 0.5 vol.% O<sub>2</sub> balanced with N<sub>2</sub> was supplied at a flow rate of 20 mL/min into the reactor. The operating pressure was 1 atm. Oxygen and nitrogen in the mixture were measured by mass flowmeters. The reaction temperature was controlled at 26–45 °C. The products were qualified by a GC–MS and a LC–MS

in batches and quantified online by a Shimadzu GC 2014C equipped with a FID detector.

The methanol conversion was obtained, assuming the volumetric flow rate was constant before and after the reaction due to the low reactant content in the feed gas, by the equation

$$C = \frac{\rho_{M0} - \rho_{M1}}{\rho_{M0}} \times 100\%, \quad (1)$$

where  $C$  is the methanol conversion, %;  $\rho_{M0}$  is the initial methanol content, mg L<sup>-1</sup>; and  $\rho_{M1}$  is the methanol content in the gas after reaction, mg L<sup>-1</sup>. The selectivity of MF was calculated by the equation

$$S = \frac{2\rho_{MF}}{\rho_{M0} - \rho_{M1}} \times 100\%, \quad (2)$$

where  $S$  is the MF selectivity, %, and  $\rho_{MF}$  is the MF content in the gas after reaction, mg L<sup>-1</sup>. The yield of MF was calculated by the equation

$$Y = C \times S \times 100\%, \quad (3)$$

where  $Y$  is the yield of MF, %;  $C$  is the methanol conversion, %; and  $S$  is the MF selectivity, %.

## 3. Results and discussion

The TEM images of 7Cu/H-ZnO-5(3), 7Cu/H-ZnO-5(7), and 7Cu/H-ZnO-5(8) are shown in Fig. 2a–c. The sheetlike structures are CuZnAl hydrotalcites and the spherulike structures are ZnO nanoparticles. Most of the ZnO nanoparticles are wrapped by the

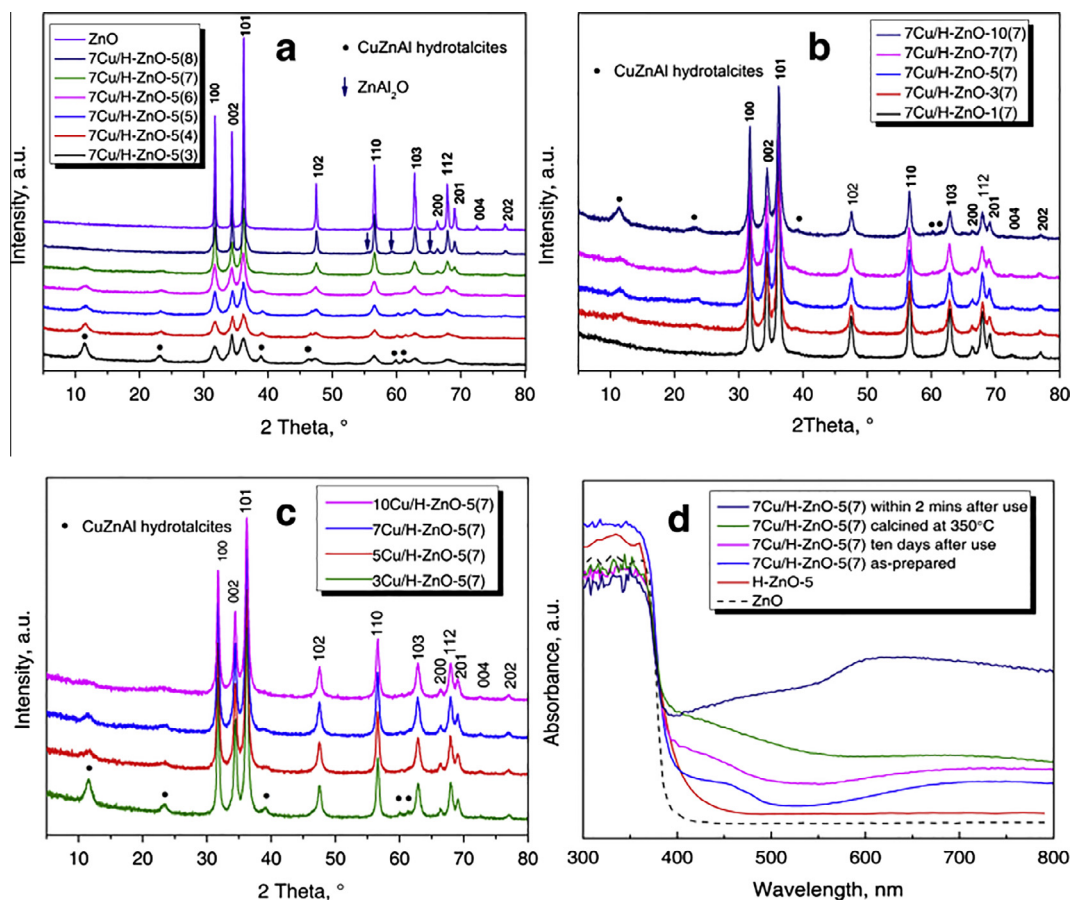


Fig. 3. XRD profiles of catalysts: effect of calcination temperature (a), Al content (b), and Cu content (c). UV-vis spectra of catalysts (d).

sheets of hydrothermalites in the samples calcined at low temperatures (Fig. 2a), and more and more of them are exposed in the samples calcined at higher temperatures (Fig. 2b and c). The influence of Al and Cu content on the morphology of the catalyst is shown in Figs. S1–S7 in the Electronic Supplementary Information. The amount of hydrothermalites in the catalyst increases with the increase in Al content but with the decrease in Cu content. The inset of Fig. 2b (image enlarged can also be seen in Fig. S8) shows the HRTEM image of the as-prepared 7Cu/H-ZnO-5(7). The distances between (100) facets of ZnO, between (012) facets of hydrothermalite, and between (111) facets of CuO are clearly distinguished. The crystal of ZnO is in close contact with that of hydrothermalite. The HRTEM image of the used 7Cu/H-ZnO-5(7) obtained within 2 min after catalysis is shown in Fig. 2d. The status of the species observed in the image is considered to be similar to that in the catalyst in the working state. The close contact interface formed by the three phases of ZnO, hydrothermalite, and metallic Cu can be observed clearly. Almost everywhere there are hydrothermalites there are such interfaces, because hydrothermalites are developed on Al-doped ZnO and CuO.

The XRD profiles of the catalysts are shown in Fig. 3a–c. The diffractions from hexagonal ZnO (PDF code: 00-001-1136) and rhombohedral hydrothermalites (PDF code: 00-037-0629 or 00-038-0487) can be identified in most of the samples and the amount of hydrothermalites in the catalyst decreases as the calcination temperature is raised from 300 to 800 °C (Fig. 3a). Only a very small amount of hydrothermalites exists in 7Cu/H-ZnO-5(7), and no hydrothermalites, but ZnAl<sub>2</sub>O<sub>4</sub> instead, are observed in 7Cu/H-ZnO-5(8). The sample 7Cu/H-ZnO-5(8) was prepared using the same recipe under the same condition as other 7Cu/H-ZnO-5(x) samples, except that

the support H-ZnO-5 was calcined at 800 °C. However, its morphology (Fig. 2c) is quite different from that of other samples. No sheetlike hydrothermalites can be observed. The XRD result provides the same evidence that no hydrothermalites, but rather ZnAl<sub>2</sub>O<sub>4</sub> is, exist in this sample. It indicates that the structure of ZnAl<sub>2</sub>O<sub>4</sub> is stable, and cannot react with copper species to give rise to hydrothermalites at the second step of loading Cu species during the preparation. At constant Cu and Zn content, the amount of hydrothermalites in the catalyst increases with increasing Al content (Fig. 3b), but it decreases with increasing Cu content at constant Al and Zn content (Fig. 3c). This seemingly abnormal phenomenon might correlate with thermodynamic equilibrium of the preparing system: copper species tend to grow together in the case of high Cu content. Copper species cannot be detected from the XRD patterns, and are hardly observed from the HRTEM images except in the samples with high Cu content. This is because some Cu is involved in the formation of hydrothermalites.

Fig. 3d shows the UV-vis spectra of catalysts. The band gap of ZnO is 3.16 eV and that of H-ZnO-5(7) is 2.99 eV, calculated by the method in the literature [35,60]. The absorption band from 80 to 600 nm is attributed to the *d-d* transition of Cu<sup>2+</sup> [61,62] and that from 51 to 410 nm is attributed to charge transfer from the valence band to the conduction band of Cu oxides. Combined with the results of HRTEM and the following XPS, this indicates that CuO exists in the as-prepared 7Cu/H-ZnO-5(7), as well as in 7Cu/H-ZnO-5(7) calcined at 350 °C. The absorption band centered at 600 nm for the used 7Cu/H-ZnO-5(7), obtained within 2 min after catalysis, is attributed to the local surface plasma resonance effect (LSPR) of Cu [63], suggesting that CuO was reduced to metallic Cu under UV irradiation during the reaction. However, in the

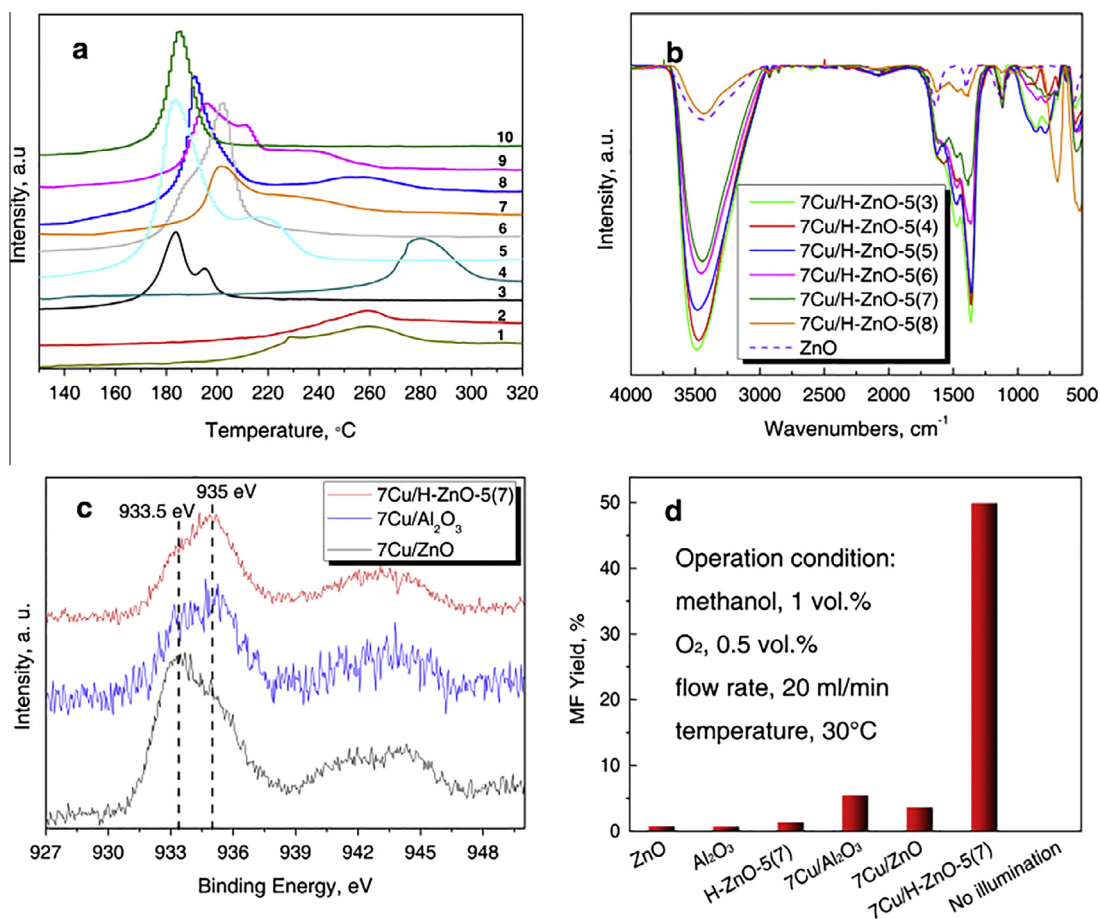


**Fig. 4.** H<sub>2</sub> TRP profiles of catalysts: (a) 1. Used catalyst tested within 2 min after catalysis; 2. 7Cu/Al<sub>2</sub>O<sub>3</sub>; 3. 7Cu/ZnO; 4. 3Cu/H-ZnO-5(7); 5. 10Cu/H-ZnO-5(7); 6. 7Cu/H-ZnO-1(7); 7. 7Cu/H-ZnO-10(7); 8. 7Cu/H-ZnO-5(3); 9. 7Cu/H-ZnO-5(7); 10. 7Cu/H-ZnO-5(8). FTIR spectra of catalysts calcined at different temperatures (b). XPS spectra of catalysts (c). Activity of reference catalysts and blank experiment (d).

sample of used 7Cu/H-ZnO-5(7) 10 days after catalysis in air, the characteristic absorbance of CuO is recovered instead of the LSPR absorbance from metallic Cu. The color change from the original light cyan of the as-prepared catalyst to the light slate gray of the used catalyst indicates the variation of Cu species from another angle.

The variation of Cu species in catalysts can also be understood from the H<sub>2</sub> TPR profiles in Fig. 4a. The reduction bands at temperatures lower than 200 °C are ascribed to the reduction of CuO nanoparticles [64,65]. The bands at temperatures higher than 200 °C are ascribed to the Cu species strongly interacting with Al<sub>2</sub>O<sub>3</sub> or to the CuZnAl hydrotalcites [66,67]. The reduction profile of CuO on ZnO (curve 3 in Fig. 4a) indicates that CuO nanoparticles are isolated and almost no interaction occurs between them. The peak at the lower-temperature band is ascribed to the reduction of highly dispersed CuO species and the shoulder at the higher-temperature band is ascribed to that of larger CuO nanoparticles. The reduction temperature of CuO on Al<sub>2</sub>O<sub>3</sub> is 80 °C higher than that on ZnO (curve 2 in Fig. 4a), indicating a strong interaction between them. With increasing Cu loading at constant Al and Zn content (curves 4, 9, and 5 in Fig. 4a), the reduction temperature of Cu species gradually decreases due to more and more isolated CuO nanoparticles being formed. With increasing Al loading at constant Cu and Zn content (curves 6, 9, and 7 in Fig. 4a), the reduction peaks attributed to CuO decrease but those attributed to Cu species that are hard to reduce increase due to the formation of hydrotalcites (XRD profile in Fig. 3b). At constant Cu, Zn, and Al content (curves 8, 9, and 10 in Fig. 4a), the amount of Cu species that are

hard to reduce decreases but that of CuO increases with increasing calcination temperature due to the decrease of the hydrotalcite content in catalysts (XRD profile in Fig. 3a). The catalyst 7Cu/H-ZnO-5(8) only shows the reduction band of CuO due to the high calcination temperature, while the used 7Cu/H-ZnO-5(7) (curve 1 in Fig. 4a) gives only the reduction band attributed to Cu species in hydrotalcites, performed within 2 min after catalysis, suggesting that CuO was reduced to metallic Cu but the Cu species in hydrotalcites were preserved well during the reaction. This result is consistent with that of UV-vis spectroscopy.

Fig. 4b shows the FTIR spectra of 7Cu/H-ZnO-5(z) and ZnO. There are very few hydroxyls on the surface of ZnO. Most of the hydroxyls on the catalyst come from hydrotalcites. The bands ranging from 3700 to 2900 cm<sup>-1</sup> originate from the O–H stretching vibrations, including those from absorbed water and hydroxyls on the surfaces of hydrotalcites [23,31]. The bands around 1370 cm<sup>-1</sup> are ascribed to the stretching vibrations of COO<sup>-</sup> and C–OH. Both of these two bands decrease with increasing calcination temperature. 7Cu/H-ZnO-5(8) shows the smallest absorption from 3700 to 2900 cm<sup>-1</sup>, indicating very few hydroxyls in this sample. The absorption in this band is strengthened with increasing Al content, but varies slightly with changing Cu content (Figs. S10 and S11, Electronic Supplementary Information).

Fig. 4c shows the core-level XPS spectra of Cu 2p<sub>3/2</sub> from 7Cu/ZnO, 7Cu/Al<sub>2</sub>O<sub>3</sub>, and 7Cu/H-ZnO-5(7). The binding energy (BE) peak (shoulders for 7Cu/Al<sub>2</sub>O<sub>3</sub> and 7Cu/H-ZnO-5(7)) located at 933.5 eV from the three catalysts is ascribed to the Cu 2p<sub>3/2</sub> from Cu<sup>2+</sup> in CuO [68–70]. However, the peaks (shoulder for 7Cu/ZnO)

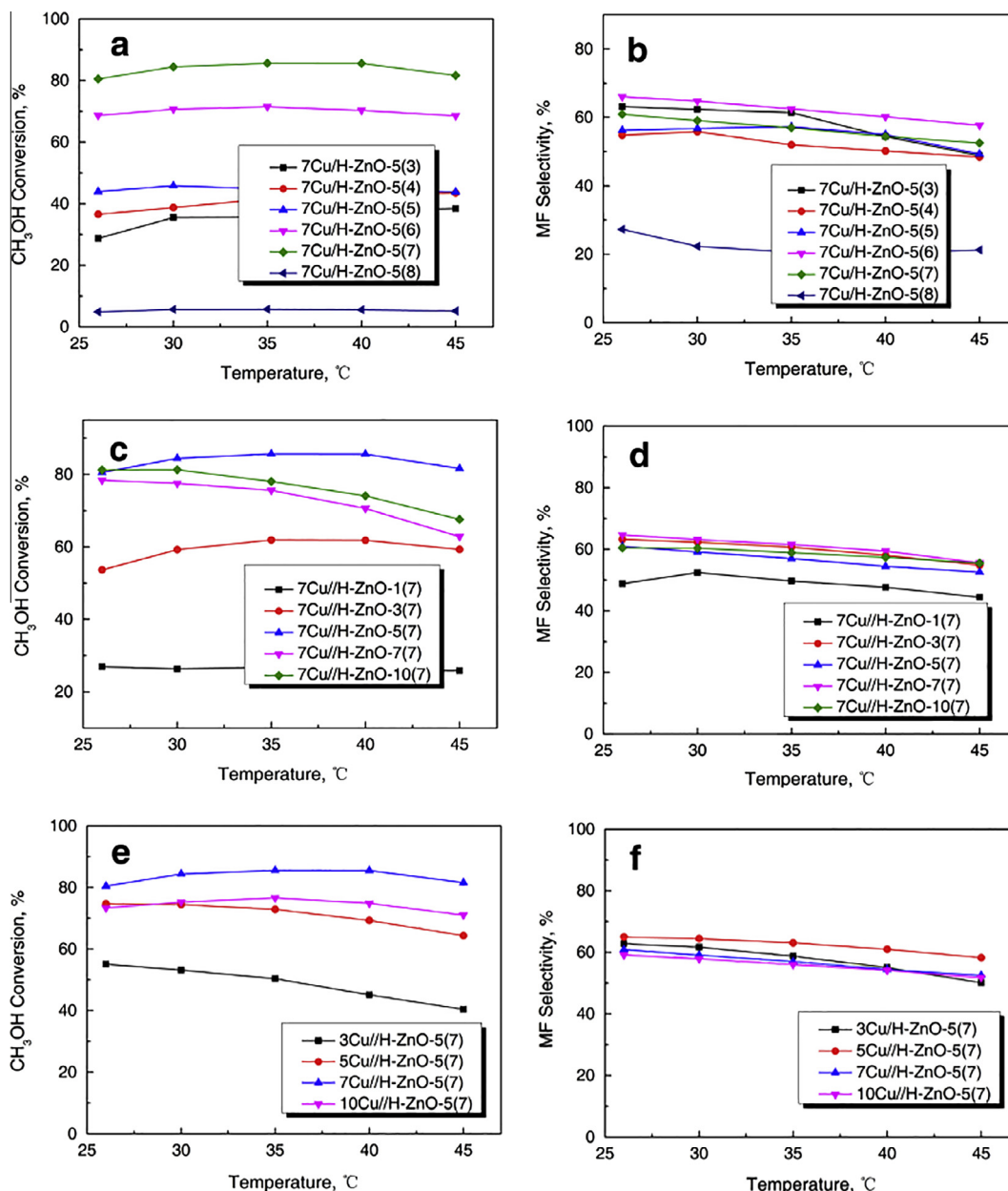


Fig. 5. Methanol conversion and MF selectivity of catalyst: 7Cu/H-ZnO-5(z) (a and b); 7Cu/H-ZnO-y(7) (c and d); xCu/H-ZnO-5(7) (e and f).

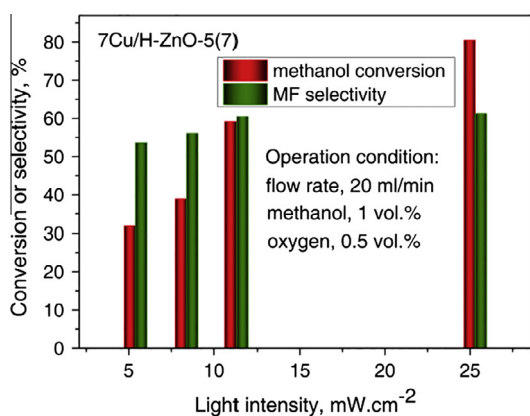


Fig. 6. Influence of light intensity on photocatalytic performance.

located at 935.0 eV are ascribed to Cu<sup>2+</sup> in different Cu species, from CuZnAl hydrotalcites for 7Cu/H-ZnO-5(7) but from CuO interacting with hydroxyls for 7Cu/Al<sub>2</sub>O<sub>3</sub> and 7Cu/ZnO [70]. The hydroxyls originate from water solution during the loading of Cu. The bands around 944 eV are ascribed to the shakeup satellite peaks of Cu<sup>2+</sup> related to an open 3d<sup>9</sup> shell. The XPS results indicate that less CuO exists in 7Cu/H-ZnO-5(7) and 7Cu/Al<sub>2</sub>O<sub>3</sub> than in 7Cu/ZnO, which is consistent with the results of H<sub>2</sub> TPR investigation.

The MF yields on ZnO, Al<sub>2</sub>O<sub>3</sub>, H-ZnO-5(7), 7Cu/Al<sub>2</sub>O<sub>3</sub>, 7Cu/ZnO, and 7Cu/H-ZnO-5(7) at 30 °C under or without UV irradiation are shown in Fig. 4d. None of these catalysts showed any photocatalytic activity without UV irradiation. The bare ZnO and Al<sub>2</sub>O<sub>3</sub> exhibit negligible activity for this reaction under UV irradiation, while H-ZnO-5(7) is slightly better than either ZnO or Al<sub>2</sub>O<sub>3</sub>. However, the MF yields are remarkably enhanced after loading Cu, up to 5.4%, 3.6%, and 49.9% for 7Cu/Al<sub>2</sub>O<sub>3</sub>, 7Cu/ZnO, and 7Cu/H-ZnO-5(7), respectively. The photocatalytic activities of catalysts prepared

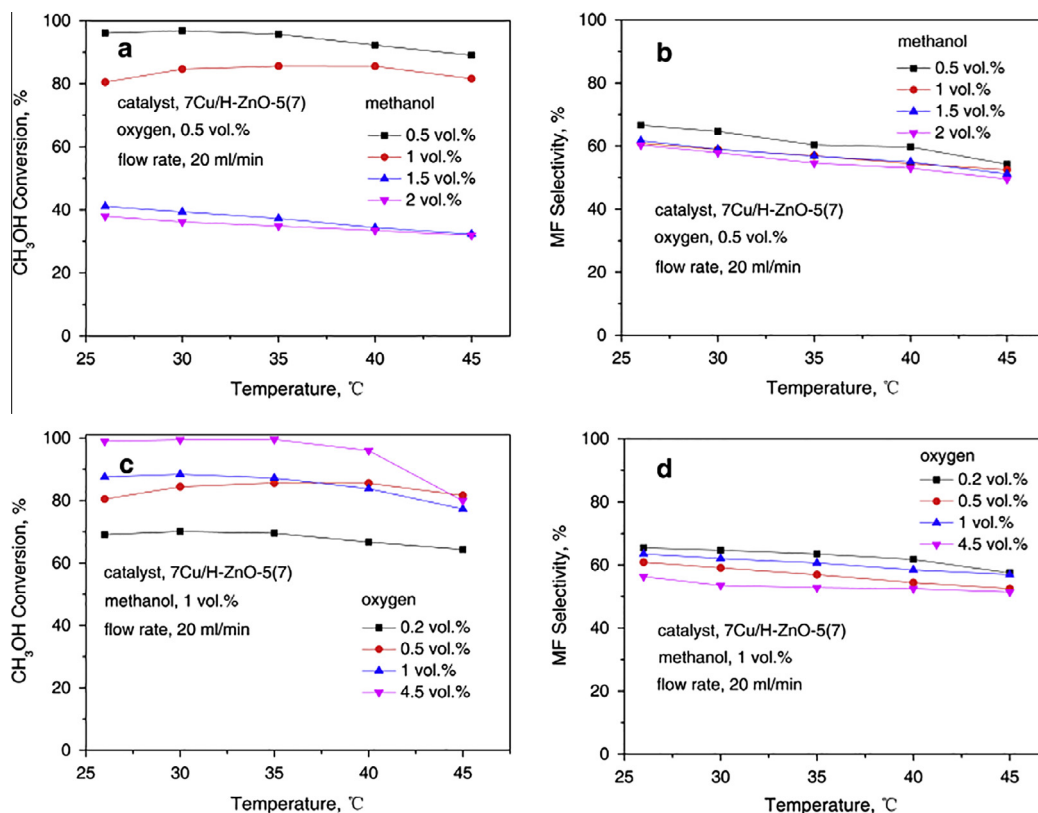


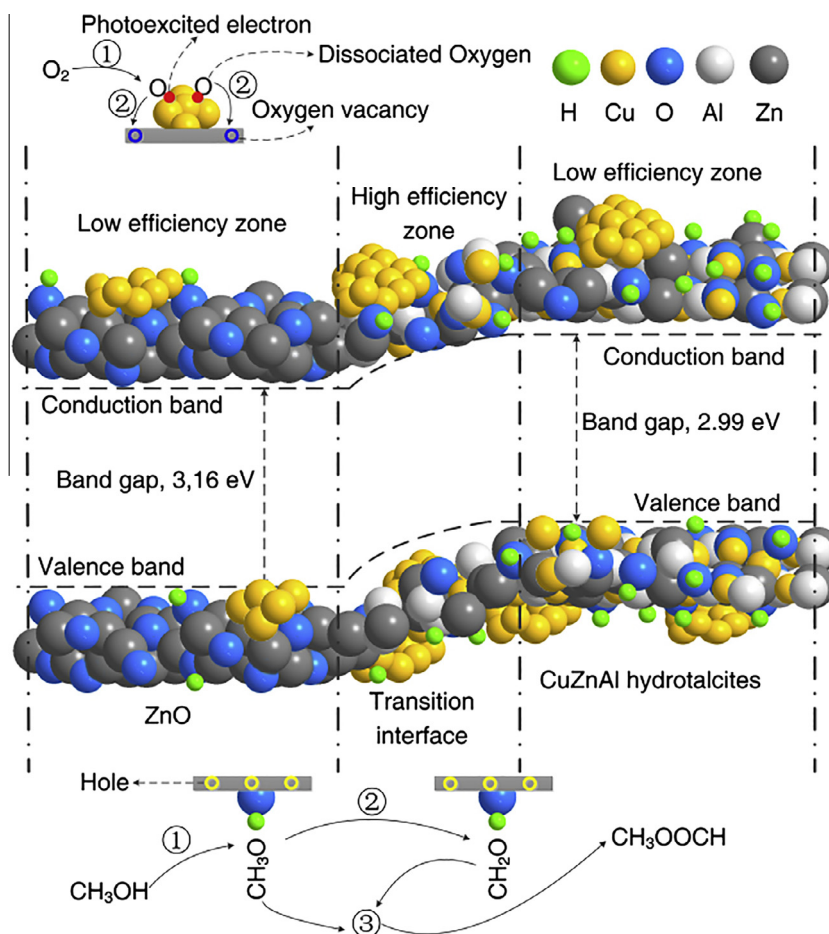
Fig. 7. Influence of methanol partial pressure in raw flow gas (a and b); influence of oxygen partial pressure in raw flow gas (c and d).

under different conditions for selective oxidation of methanol to MF under UV irradiation in the temperature range from 26 to 45 °C are shown in Fig. 5. No by-products other than CO<sub>2</sub> can be definitely detected for all of the catalysts. The methanol conversion changes slightly, but the MF selectivity decreases gradually with increasing reaction temperature from 26 to 45 °C for most of the catalysts. The catalyst 7Cu/H-ZnO-5(7) exhibits the maximum MF yield of 49.9% at methanol conversion of 84.5% and MF selectivity of 59.1% at 30 °C. At a constant molar ratio of Cu:Zn:Al (Fig. 5a and b), the methanol conversion increases, from 35.5% to 84.5% at 30 °C with increasing calcination temperature from 300 to 700 °C, and the selectivity of the catalyst varies slightly. But the methanol conversion and MF selectivity dramatically decrease if the calcination temperature is at 800 °C, from 84.5% to 5.7% and from 59.1% to 22.3%, respectively, at a reaction temperature of 30 °C. At a constant molar ratio of Cu to Zn and calcination temperature (Fig. 5c and d), the methanol conversion increases from 26.3% to 84.5% at 30 °C with the increase of Al content from 1% to 5%, but the methanol conversion and MF selectivity decrease slightly at Al content higher than 5%. The MF selectivity is parallel for the catalyst with Al content higher than 5%. At constant molar ratio of Zn to Al and calcination temperature (Fig. 5e and f), the methanol conversion increases from 53.2% to 84.5% at 30 °C with the increase of Cu loading from 3% to 7%, but it decreases from 84.5% to 75.3% at 30 °C when the Cu content is up to 10%. The selectivity of the catalyst with different Cu content varies slightly from 26 to 45 °C. But the catalysts with low Cu content exhibit slightly better MF selectivity.

The influence of the light intensity on the catalytic performance of 7Cu/H-ZnO-5(7) is shown in Fig. 6. The methanol conversion increases sharply and almost linearly, but the MF selectivity increases slightly with increased light intensity from 5.4 to 25.3 mW cm<sup>-2</sup>.

The influence of methanol partial pressure and oxygen partial pressure on the photocatalytic performance of 7Cu/H-ZnO-5(7) is shown in Fig. 7. The methanol conversion decreases sharply from ca. 100% to ca. 40% with increasing methanol concentration from 0.5 to 2.0 vol.% at oxygen concentration 0.5 vol.%. The MF selectivity changes slightly with the change in the methanol concentration. The methanol conversion increases greatly from ca. 70% to ca. 100% with the increase of oxygen concentration from 0.2 to 4.5 vol.% at a methanol concentration of 1 vol.%, and the MF selectivity decreases with increasing oxygen concentration. According to the MF formation rate, the optimum ratio of methanol to oxygen is 2:1 and the optimum methanol concentration is 1 vol.% for this catalyst.

The bare ZnO and Cu/ZnO exhibit inferior photocatalytic activity for the selective oxidation of methanol to MF, although the band gap energy, valence band maximum, and conduction band minimum are almost similar to those of titania. This is because there are few hydroxyls on the surface of ZnO, which are essential to forming methoxy by reacting with methanol molecules. From methanol to methoxy is the key step of the reaction [3,7,8]. From the results of catalysis, the samples with high content of hydroxyls such as 7Cu/H-ZnO-5(3) and 3Cu/H-ZnO-5(7) usually exhibit poor photocatalytic performance, indicating that hydroxyls are not active for this reaction, although there are plenty of hydroxyls on their surfaces. This is because the valence band maximum of CuZnAl hydroxalicates is slightly higher than that of ZnO, and thus the redox potential of the photoexcited holes on the surface of hydroxalicates is slightly negative or similar to that of CH<sub>3</sub>O<sup>-</sup>/CH<sub>2</sub>O<sup>-</sup>, against further oxidation of methoxy to coordinated formaldehyde. On the other hand, catalysts without hydroxalicates, such as 7Cu/H-ZnO-5(8), exhibit the worst photocatalytic activity for this reaction, while the best photocatalyst for selective oxidation of methanol to MF is 7Cu/H-ZnO-5(7), a nanocomposite with CuO



**Scheme 1.** Proposed reaction mechanism of selective oxidation of methanol to MF on the catalyst CuO supported on CuZnAl hydrotalcites and ZnO nanocomposite.

of 7% supported on ZnO and a suitable amount of hydrotalcites. So we believe that the interface between ZnO and CuZnAl hydrotalcites must play an important role in the reaction.

Both ZnO and CuZnAl hydrotalcites are semiconductors. When they electronically contact with each other the band bending/heterojunction is formed at the interface between ZnO and CuZnAl hydrotalcites in order to maintain aligned Fermi level [13]. The valence band maximum at the interface is higher than that of ZnO but lower than that of hydrotalcites, leading to the redox potential of the photogenerated holes at the heterojunction close to the side of ZnO being more positive than that of  $\text{CH}_3\text{O}^-/\text{CH}_2\text{O}^-$ . On the other hand, the outer surface around the interface has plenty of hydroxyls from hydrotalcites. These two aspects make the zone of the interface between ZnO and CuZnAl hydrotalcites more effective for the selective oxidation of methanol to MF under UV irradiation. The proposed mechanism of the reaction is shown in Scheme 1.

#### 4. Conclusions

A novel catalyst of CuO supported on ZnO and CuZnAl hydrotalcites has been prepared using cheap raw materials and a simple wet chemical method. The catalyst exhibits remarkable photocatalytic activity for selective oxidation of methanol to MF. The interfaces of ZnO, CuZnAl hydrotalcite, and Cu species in the catalyst play an important role in the reaction. Hydrotalcites are not very active in the reaction but supply hydroxyls in the high-efficiency zone near the interface. The amount of hydrotalcites in catalysts can be controlled by modulating the calcination temperature and

the Al and Cu content. CuO is reduced to metallic Cu during the reaction, which plays a role in the dissociation of oxygen. This study provides new insights into the design of photocatalysts for selective oxidation of methanol to MF.

#### Acknowledgments

This work was financially supported by the National Natural Science Foundation of China (No. 21566026), a key project of the Inner Mongolia Education Department, China (NJZZ13002), the Natural Science Foundation of Inner Mongolia, China (2014MS0207), a project of Grassland Talent of Inner Mongolia, China and a project of the western light from the ODP of Inner Mongolia, China.

#### Appendix A. Supplementary material

Supplementary data associated with this article can be found, in the online version, at <http://dx.doi.org/10.1016/j.jcat.2016.03.033>.

#### References

- [1] S.P. Tonner, D.L. Trimm, M.S. Wainwright, N.W. Cant, *Ind. Eng. Chem. Prod. Res. Dev.* 23 (1984) 384.
- [2] E. Tronconi, A.S. Elmi, N. Ferlazzo, P. Forzatti, *Ind. Eng. Chem. Res.* 26 (1987) 1269.
- [3] A.S. Elmi, E. Tronconi, C. Cristiani, J.P. Gomez Martin, P. Forzatti, *Ind. Eng. Chem. Res.* 28 (1989) 387.
- [4] M. Ai, *J. Catal.* 77 (1982) 279.
- [5] H. Liu, E. Iglesia, *J. Phys. Chem. B* 109 (2005) 2155.

- [6] A. Wittstock, V. Zielasek, J. Biener, C.M. Friend, M. Bäumer, *Science* 327 (2010) 319.
- [7] C. Han, X. Yang, G. Gao, J. Wang, H. Lu, J. Liu, M. Tong, X. Liang, *Green Chem.* 16 (2014) 3603.
- [8] J. Liu, C. Han, X. Yang, G. Gao, Q. Shi, M. Tong, X. Liang, C. Li, *J. Catal.* 333 (2016) 162.
- [9] X. Yang, A. Zhang, G. Gao, D. Han, C. Han, J. Wang, H. Lu, J. Liu, M. Tong, *Catal. Commun.* 43 (2014) 192.
- [10] J.C. Colmenares, P. Lisowski, D. Łomot, O. Chernyayeva, D. Lisovyskiy, *ChemSusChem* 8 (2015) 1676.
- [11] H. Kominami, H. Sugahara, K. Hashimoto, *Catal. Commun.* 11 (2010) 426.
- [12] Y. Liu, G. Griffin, S. Chan, I. Wachs, *J. Catal.* 94 (1985) 108.
- [13] A.L. Linsebigler, G. Lu, J.T. Yates Jr., *Chem. Rev.* 95 (1995) 735.
- [14] C. Tian, Q. Zhang, A. Wu, M. Jiang, Z. Liang, B. Jiang, H. Fu, *Chem. Commun.* 48 (2012) 2858.
- [15] C. Hariharan, *Appl. Catal. A* 304 (2006) 55.
- [16] A. Akyol, H.C. Yatmaz, M. Bayramoglu, *Appl. Catal. B: Environ.* 54 (2004) 19.
- [17] G. Mahmodi, S. Sharifnia, F. Rahimpour, S.N. Hosseini, *Sol. Energy Mater.: Sol. Cells* 111 (2013) 31.
- [18] R. Ullah, J. Dutta, *J. Hazard. Mater.* 156 (2008) 194.
- [19] A.P. Bhirud, S.D. Sathaye, R.P. Waichal, L.K. Nikam, B.B. Kale, *Green Chem.* 14 (2012) 2790.
- [20] M. Francavilla, A. Pineda, A.A. Romero, J.C. Colmenares, C. Vargas, M. Monteleone, R. Luque, *Green Chem.* 16 (2014) 2876.
- [21] N. Ahmed, Y. Shibata, T. Taniguchi, Y. Izumi, *J. Catal.* 279 (2011) 123.
- [22] D. Carriazo, M. del Arco, E. García-López, G. Marcí, C. Martín, L. Palmisano, V. Rives, *J. Mol. Catal. A* 342–343 (2011) 83.
- [23] M.A. Larrubia Vargas, G. Busca, U. Costantino, F. Marmottini, T. Montanari, P. Patrono, F. Pinzari, G. Ramis, *J. Mol. Catal. A* 266 (2007) 188.
- [24] S. Nishimura, A. Takagaki, K. Ebitani, *Green Chem.* 15 (2013) 2026.
- [25] P. Roy Chowdhury, K.G. Bhattacharyya, *Dalton Trans.* 44 (2015) 6809.
- [26] Y. Zhi, Y. Li, Q. Zhang, H. Wang, *Langmuir* 26 (2010) 15546.
- [27] E.M. Seftel, E. Popovici, M. Mertens, K.D. Witte, G.V. Tendeloo, P. Cool, E.F. Vansant, *Micropor. Mesopor. Mater.* 113 (2008) 296.
- [28] S.-M. Xu, T. Pan, Y.-B. Dou, H. Yan, S.-T. Zhang, F.-Y. Ning, W.-Y. Shi, M. Wei, *J. Phys. Chem. C* 119 (2015) 18823.
- [29] Y. Lee, J.H. Choi, H.J. Jeon, K.M. Choi, J.W. Lee, J.K. Kang, *Energy Environ. Sci.* 4 (2011) 914.
- [30] R. Lu, X. Xu, J. Chang, Y. Zhu, S. Xu, F. Zhang, *Appl. Catal. B* 111–112 (2012) 389.
- [31] G. Carja, A. Nakajima, S. Dranca, C. Dranca, K. Okada, *J. Phys. Chem. C* 114 (2010) 14722.
- [32] E.M. Seftel, M. Mertens, P. Cool, *Appl. Catal. B* 134–135 (2013) 274.
- [33] J.S. Valente, F. Tzompantzi, J. Prince, *Appl. Catal. B* 102 (2011) 276.
- [34] F.P. Koffyberg, *J. Appl. Phys.* 53 (1982) 1173.
- [35] Y. Xu, M.A. Schoonen, *Am. Mineral.* 85 (2000) 543.
- [36] D. Praveen Kumar, M.V. Shankar, M.M. Kumari, G. Sadanandam, B. Srinivas, V. Durgakumari, *Chem. Commun.* 49 (2013) 9443.
- [37] Z. Wang, Y. Liu, D.J. Martin, W. Wang, J. Tang, W. Huang, *Phys. Chem. Chem. Phys.* 15 (2013) 14956.
- [38] C. Ampelli, R. Passalacqua, C. Genovese, S. Perathoner, G. Centi, T. Montini, V. Gombac, J.J. Delgado Jaen, P. Fornasiero, *RSC Adv.* 3 (2013) 21776.
- [39] M. Hara, T. Kondo, M. Komoda, S. Ikeda, K. Shinohara, A. Tanaka, J.N. Kondo, K. Domen, *Chem. Commun.* 3 (1998) 357.
- [40] X. An, K. Li, J. Tang, *ChemSusChem* 7 (2014) 1086.
- [41] P.D. Tran, L.H. Wong, J. Barber, J.S.C. Loo, *Energy Environ. Sci.* 5 (2012) 5902.
- [42] H. Li, Y. Lei, Y. Huang, Y. Fang, Y. Xu, L. Zhu, X. Li, *J. Nat. Gas Chem.* 20 (2011) 145.
- [43] X. Hua, O. Shuxin, L. Lequan, W. Defa, K. Tetsuya, Y. Jinhua, *Nanotechnology* 25 (2014) 165402.
- [44] X. Li, J. Wen, J. Low, Y. Fang, J. Yu, *Sci. China Mater.* 57 (2014) 70.
- [45] A.D. Handoko, J. Tang, *Int. J. Hydrogen Energy* 38 (2013) 13017.
- [46] Z. Xiong, L.L. Zhang, X.S. Zhao, *Chemistry* 17 (2011) 2428.
- [47] H.-Y. Jing, T. Wen, C.-M. Fan, G.-Q. Gao, S.-L. Zhong, A.-W. Xu, *J. Mater. Chem. A* 2 (2014) 14563.
- [48] P.E. de Jongh, D. Vanmaekelbergh, J.J. Kelly, *Chem. Commun.* (1999) 1069.
- [49] A.V. Walker, J.T. Yates, *J. Phys. Chem. B* 104 (2000) 9038.
- [50] A. Paracchino, V. Laporte, K. Sivula, M. Grätzel, E. Thimsen, *Nat. Mater.* 10 (2011) 456.
- [51] K. Jacobi, G. Zwicker, A. Gutmann, *Surf. Sci.* 141 (1984) 109.
- [52] H.B. Michaelson, *J. Appl. Phys.* 48 (1977) 4729.
- [53] V. Russier, J. Badiali, *Phys. Rev. B* 39 (1989) 13193.
- [54] I. Paramasivam, J.M. Macak, P. Schmuki, *Electrochem. Commun.* 10 (2008) 71.
- [55] V. Iliev, D. Tomova, L. Bilyarska, A. Eliyas, L. Petrov, *Appl. Catal. B* 63 (2006) 266.
- [56] Z. Ji, M.N. Ismail, D.M. Callahan, E. Pandowo, Z. Cai, T.L. Goodrich, K.S. Ziemer, J. Warzywoda, A. Sacco, *Appl. Catal. B* 102 (2011) 323.
- [57] A. Primo, A. Corma, H. Garcia, *Phys. Chem. Chem. Phys.* 13 (2011) 886.
- [58] A. Dawson, P.V. Kamat, *J. Phys. Chem. B* 105 (2001) 960.
- [59] M. Jakob, H. Levanon, P.V. Kamat, *Nano Lett.* 3 (2003) 353.
- [60] S. Tsunekawa, T. Fukuda, A. Kasuya, *J. Appl. Phys.* 87 (2000) 1318.
- [61] H. Irie, S. Miura, K. Kamiya, K. Hashimoto, *Chem. Phys. Lett.* 457 (2008) 202.
- [62] X. Qiu, M. Miyauchi, K. Sunada, M. Minoshima, M. Liu, Y. Lu, D. Li, Y. Shimodaira, Y. Hosogi, Y. Kuroda, *ACS Nano* 6 (2012) 1609.
- [63] A. Marimuthu, J. Zhang, S. Linic, *Science* 339 (2013) 1590.
- [64] G. Fierro, M. Lojacono, M. Inversi, P. Porta, R. Lavecchia, F. Cioci, *J. Catal.* 148 (1994) 709.
- [65] G. Fierro, M. Lojacono, M. Inversi, P. Porta, F. Cioci, R. Lavecchia, *Appl. Catal. A* 137 (1996) 327.
- [66] J.-P. Shen, C. Song, *Catal. Today* 77 (2002) 89.
- [67] S. Velu, K. Suzuki, M. Okazaki, M.P. Kapoor, T. Osaki, F. Ohashi, *J. Catal.* 194 (2000) 373.
- [68] F. Parmigiani, G. Pacchioni, F. Illas, P. Bagus, *J. Electron Spectrosc. Relat. Phenom.* 59 (1992) 255.
- [69] N. McIntyre, M. Cook, *Anal. Chem.* 47 (1975) 2208.
- [70] S. Murcia-Mascarós, R.M. Navarro, L. Gómez-Sainero, U. Costantino, M. Nocchetti, J.L.G. Fierro, *J. Catal.* 198 (2001) 338.